

pubs.acs.org/JPCC Perspective

Magnetism of Atomically Precise Gold and Doped Nanoclusters: Delocalized Spin and Interparticle Coupling

Yingwei Li and Rongchao Jin*



Cite This: J. Phys. Chem. C 2021, 125, 15773-15784

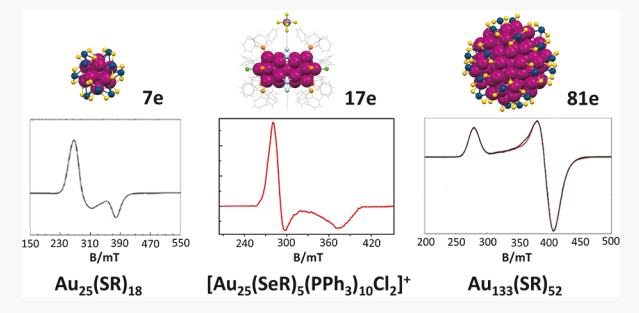


ACCESS

Metrics & More

Article Recommendations

ABSTRACT: The magnetic properties of Au nanoparticles (NPs) have long been an intriguing topic in fundamental research. In the quantum size regime (1–3 nm), Au NPs indeed exhibit distinct magnetism in contrast to diamagnetic gold in bulk or relatively large plasmonic NPs. However, previous studies often give controversial results due to imprecise NPs used in magnetic studies, making it difficult to understand the origin of magnetism in Au NPs. Recent progress has led to atomically precise Au nanoclusters (NCs for differentiation with regular NPs), which can serve as a unique model for studying the delocalized spin in isolated NCs and the spin–spin exchange interaction between NCs in assembled solids. Moreover, such



mechanisms are correlated to the atomic structures of the magnetic NCs. The precise formulas of the NCs serve as a clear indicator for magnetism. So far, the Au-thiolate NCs reported to be magnetic, including the doped ones, all contain icosahedral kernel structures, which are facile compared to other structures in adding or removing one electron for endowing magnetism to the NCs. Heteroatom doping in the NCs is an effective method to probe the magnetic mechanism in NCs, such as the origin of magnetic anisotropy, and the counterion tailoring for those charged NCs can also impart magnetism to the initially diamagnetic NCs via stabilizing a particular charge state of the NCs. While only a few cases of NCs have been reported with magnetism thus far, future research on metal NCs (especially in the critical regime between molecular and metallic state) will reveal more fundamentals of magnetism, and the control of spin—spin exchange coupling in nanocluster-assembled solids is particularly promising for tailoring the magnetic functionality of NCs and ultimately finding versatile applications.

1. INTRODUCTION

Although single gold atoms are paramagnetic because of the unpaired 6s¹ electron, bulk gold is diamagnetic as the 5d¹⁰ electrons are buried deep below the Fermi level and the orbital and ionic core diamagnetism counteracts the weak paramagnetism of conduction electrons.^{2,3} Nanoparticles and clusters of metals have intriguing physical and electronic properties due to quantum size effects.⁴ Two decades ago, some of the ligand-protected Au nanoparticles (NPs) were found to have permanent magnetism, 5-7 being different from the diamagnetic bulk Au and "naked" Au NPs (deposited from gas phase). The observed magnetism was found to be closely related to the particle size and the type of capping ligands. 8-10 Hori et al. reported ~20 spins per particle in poly(N-vinyl-2pyrrolidone) protected Au NPs of ~3 nm diameter, and such a large magnetic moment cannot be explained by the "odd/even electron number effect" and Stoner's enhancement model.⁵ Poly(allylamine hydrochloride)-stabilized Au NPs (~1.9 nm diameter) demonstrated ferromagnetic spin polarization.8 In terms of the ligand effect, dodecanethiolate-capped Au NPs were ferromagnetic and tiopronin-protected ones were paramagnetic, but tetraalkylammonium-capped ones were diamagnetic.11 Gold NPs of ~5 nm with dodecanethiolate ligands

showed a blocking temperature of ~50 K, while the ~12 nm NPs were diamagnetic. For phosphine/chloride coprotected Au NPs, it is interesting to see that permanent magnetism (measured at both 5 and 300 K) can be observed in ~2 nm NPs, but not in undecagold clusters. Unfortunately, some of these early results may be controversial, to probably due to less precise control over the composition, structure, charge state, and crystallinity of NPs. For example, in polydispersed Au NPs, the magnetism might come from one (or more) type(s) of Au NPs of specific size (or Au atom number) in the mixture, while other sizes are nonmagnetic. Besides, magnetism could be affected by impurities, and one must be very careful in sample preparation as contamination from objects like a metal spatula may lead to spurious results. Thus, these observations require more analyses. Later, the Lear group

 Received:
 May 26, 2021

 Revised:
 June 28, 2021

 Published:
 July 15, 2021





synthesized plasmonic Au–thiolate NPs with metal core diameters of 1.8-1.9 nm (highly monodispersed as indicated by transmission electronic microscopy), and managed to demonstrate that the g factors probed by conduction electron spin resonance (CESR) can be controlled by thiolates with different lengths or substituents as well as solvents with different dielectric constants. 17,18 Nevertheless, the origin of magnetism remains unclear. But a common trend is that ultrasmall Au-SR NPs within a critical size range seem the most promising ones to be responsible for the outstanding magnetic properties.

In order to identify the origin of magnetism in Au NPs, the sample should ideally contain only one size, i.e., atomically identical. Fortunately, ultrasmall Au-SR NPs with core size <3 nm have been made with atomic precision (called Au-SR nanoclusters, NCs), 19,20 with all particles in a sample being truly identical. In ultrasmall NPs, the surface plasmon resonance (SPR) band—which dominates the optical spectrum of larger Au NPs—vanishes at sizes below Au₂₇₉(SR)₈₄, giving rise to a multiband spectrum due to discrete energy states in small NCs. 21-23 Moreover, such atomically precise NCs can grow into single crystals for atomic structure determination by X-ray crystallography (SCXRD), providing ideal platforms for correlating the total structures and physicochemical properties. 19,24 As such, many fundamental issues such as the structural evolution (even atom by atom), ^{25–27} assembly, ^{28–30} isomerism, ^{31–33} optical absorption, ^{22,34} excited state dynamics, ^{35,36} chirality, ^{37–39} photoluminescence, ^{40–42} dipole moments, ⁴³ and catalytic performance, ^{44–47} as well as magnetism, ⁴⁸ have been studied. The magnetic properties of thiolate (SR) protected Au NPs hold promise in magnetic resonance imaging, magneto-optical data storage, recyclable nanocatalysts, etc., 49-51 but the fundamentals are still poorly understood. Generally, the physicochemical properties of NPs are greatly affected by their size and surface. X-ray studies revealed that, as the size of thiolate-protected NPs decreases, the d orbitals become more depleted relative to bulk gold due to Au-S charge redistribution, 52 hence, potentially giving rise to magnetism. The well-defined nanoclusters offer a model for probing the magnetism and providing insights.

In this Perspective, we highlight the magnetic properties of atomically precise Au and doped NCs. It has become clear that an odd number of core valence electrons, determined by the numbers of Au atoms, ligands, and charge state of the NC, rather than the ligand type and NC size, is the origin of magnetism. We shall start with Au₂₅(SR)₁₈ NCs as a classical model to demonstrate the magnetic properties in both the isolated state and the assembled solids with exchange coupling. The effects of doping in the core as well as the shape control of Au₂₅ (e.g., sphere vs rod) are discussed subsequently. The magnetism of larger sized Au₁₃₃(SR)₅₂ is also discussed, and finally, some future perspectives are provided. Overall, the magnetism in gold and doped NCs constitutes an attractive topic, and the development of one's capability to control spinspin exchange interaction in nanocluster-assembled solids is quite promising for not only tailoring the magnetic functionality but also finding versatile applications.

2. MAGNETISM IN [Au₂₅(SR)₁₈]^q NANOCLUSTERS

While the magnetic properties are typically measured on a superconducting quantum interference device (SQUID) magnetometer, another popular technique is electron paramagnetic resonance (EPR) spectroscopy. Briefly, EPR measures the absorption of microwave radiation by a spin, followed by spin flipping. In the presence of an external magnetic field, the Kramer's degeneracy of the spin states of an unpaired electron is lifted. The applied static field B and microwave frequency (ν) are linked by the relation: $h\nu = g\mu_B B$ (where, h is the Planck constant, g is the gyromagnetic factor (g-factor), and μ_B is the Bohr magneton). EPR is a highly sensitive technique for probing materials ranging from organic free radicals to nanoparticles with surface ligands modified by radicals, and not only the paramagnetism but also ferromagnetism and superparamagnetism (see section 2.2) can be analyzed by EPR. In early times, it was suggested that Au NPs protected by self-assembled monolayers were EPR inactive; thus, paramagnetic molecules with unpaired electrons (e.g., nitroxyl radicals) were usually introduced onto the Au NPs as spin labels, and the ERP signal of the paramagnetic radical can be seen by EPR. 53-56 Note that the EPR hyperfine structure observed in radical solutions may be lost in radical-modified Au surfaces due to significant intermolecular exchange interactions typical for concentrated spin systems.⁵⁰

The EPR active $[Au_{25}(SR)_{18}]^0$ (its neutral charge highlighted for differentiation with the EPR silent anionic $[Au_{25}(SR)_{18}]^{-}$, 57 serves as a paradigm for understanding the origin of paramagnetism in atomically precise NCs (see section 2.1) as well as the exchange coupling between NCs in the assembled crystal (see section 2.2). Experimentally, three charge states of $[Au_{25}(SR)_{18}]^q$ (q = -1, 0, +1) were found to be stable. Their particular stability was earlier attributed to the geometry of [Au₂₅(SR)₁₈]^q, rather than the electron shell closing.⁵⁸ Later, a superatom picture was proposed on the basis of several cases of ligand-protected Au and Ag NCs, 59 including $[Au_{25}(SR)_{18}]^{-,60}$ $Au_{102}(SR)_{44}$, 61 and $[Ag_{44}(SR)_{30}]^{4-,62}$ According to the density functional theory (DFT) calculations on $[Au_{25}(SR)_{18}]^q$, the anionic form (q =-1) was found to have an enhanced stability originated from the eight electrons (25 - 18 + 1 = 8e), i.e., shell closing of delocalized Au(6s) electrons in the kernel of the NC.⁶³ Kohn– Sham orbitals and corresponding energies show triple degeneracy of the HOMO, with its projection being mainly of P-character, hence, the 1S²1P⁶ superatomic configuration for $[Au_{25}(SR)_{18}]^{-}$.

2.1. Superatomic Magnetism in [Au₂₅(SR)₁₈]^q Nano**clusters.** It was discovered that, as the anionic $[Au_{25}(SR)_{18}]^{-}$ NC was oxidized (e.g., reaction with 33% aqueous H_2O_2), neutral $[Au_{25}(SR)_{18}]^0$ (7e) with one unpaired electron in the P-character superatomic orbital resulted, and its rhombic EPR signal can be readily assigned.⁵⁷ The crystal structure was solved by SCXRD, 64 which contains an icosahedral Au₁₃ kernel and six staple motifs of -SR-Au-SR-Au-SR- arranged in an octahedral symmetry (Figure 1a, inset), the same to its 8e counterpart. The low-temperature EPR spectra (Figure 1a) of both microcrystalline phase and frozen solution samples demonstrate an $S = \frac{1}{2}$ signal with g = (2.56, 2.36, 1.82), gstrain $(\sigma_g) = 0.03$, and 13 equiv $I = \frac{3}{2}$ gold nuclei with hyperfine constant A = (71, 142, 50) MHz. The solvents and concentrations of the frozen solutions show no discernible change to the g values or the line width.⁵⁷

Quantification indicates that $[Au_{25}(SR)_{18}]^0$ has one unpaired spin per NC. Thus, whether an atomically precise NC is EPR active depends on whether the electron count of the NC is an odd number. The electron count is calculated by the total number of s orbital valence electrons of metal atoms

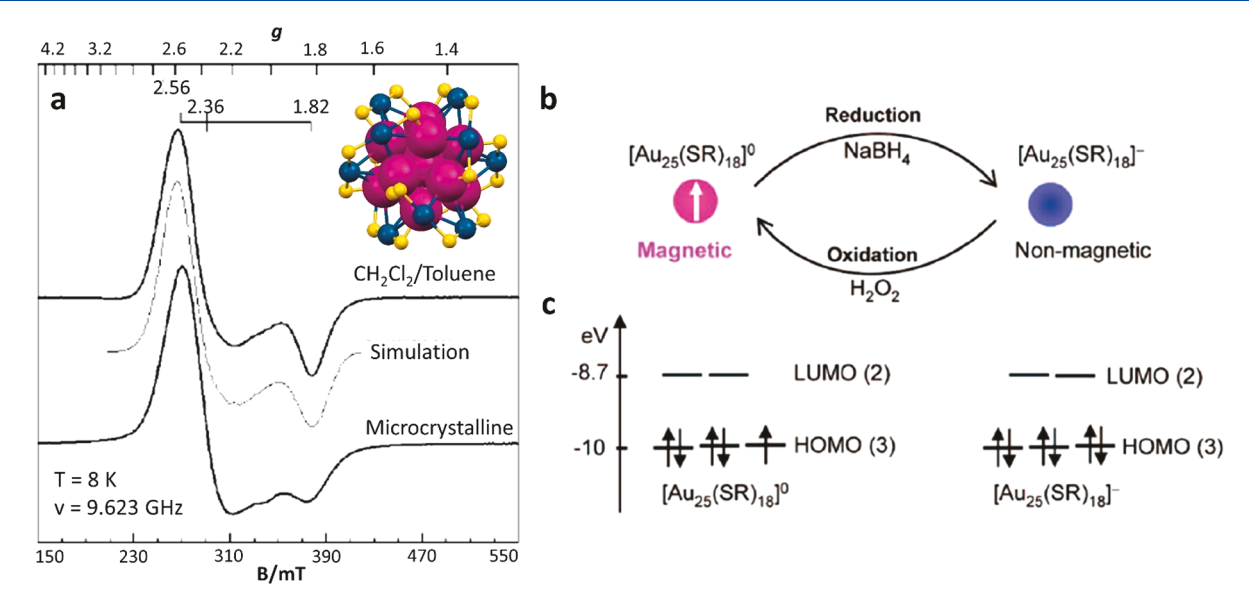


Figure 1. (a) EPR spectra of $[Au_{25}(SR)_{18}]^0$. (b) Reversible conversion between the neutral and anionic $[Au_{25}(SR)_{18}]^{0/-}$ NCs. (c) Frontier orbital level diagrams. Inset: the structure of $Au_{25}S_{18}$ (-R groups omitted for clarity). Color codes: magenta = kernel Au; blue = surface motif Au; yellow = S. Reproduced with permission from ref 57. Copyright 2009, American Chemical Society.

(e.g., Au 6s¹) being subtracted by the number of ligands as well as the charge state. In other words, as the electron configuration of $[Au_{25}(SR)_{18}]^0$ is $(a_u)^2(a_u)^2(a_u)^1$ (HOMO set) or $1S^21P^5$ (an open-shelled superatom) (Figure 1b/c), the NC is correspondingly EPR active. The P orbital exhibits an axial symmetry. The energies of the three orbitals $(P_{x,v,z})$ are indeed slightly split (P_z being ~ 0.1 eV above $P_{x,y}$) but were viewed as quasi-degeneracy in early work since the DFTsimulated HOMO-LUMO transition in [Au₂₅(SR)₁₈] had no splitting.⁶⁰ Later DFT simulations involving bulkier -SR⁶⁵ (such as SPh, as opposed to SCH₃) or spin-orbit coupling (with just SCH₃)⁶⁶ led to a splitting of the HOMO-LUMO transition into two peaks resembling the experimental spectral feature of $[Au_{25}(SR)_{18}]^{q.67,68}$ When being applied to other cases, the electron counting rule explains the diamagnetic behavior of Au_{11} NCs,¹³ including $Au_{11}(PPh_3)_7X_3$ and $[Au_{11}(PPh_3)_8X_2]^+$ (X = Cl or Br), both being 8e superstoms ^{69,70} superatoms.

The results explicitly demonstrate that sizes and ligands are not the cause of magnetism in Au NCs (ligands might have some effect on g-tensor splitting); rather, the electron count is decisive. From this conclusion, we deduce that when the electron count of an atomically precise metal NC is an odd number according to its formula, the NC should be EPR active. For example, $\mathrm{Au_{133}(SR)_{52}}$ with 81e is indeed paramagnetic (see section 5). But unexpectedly, Fanchini and coworkers reported an EPR signal from $[\mathrm{Au_{25}(SR)_{18}}]^+$ with an even number of electrons $(6\mathrm{e})^{71}$ which is still controversial since other groups determined that this 6e NC is diamagnetic, 19,48,68 and it shows a temperature-independent response in susceptibility.

2.2. Exchange Coupling between Superatomic Spins of $[Au_{25}(SR)_{18}]^0$ in Assembled Crystals. The magnetic properties of $[Au_{25}(SR)_{18}]^0$ are sensitive to the physical state and crystallinity. The Maran group reported a detailed study. The EPR signal of a single crystal of $[Au_{25}(SR)_{18}]^0$ NCs shows very narrow peaks at 2460–2630 G (Figure 2, panels a and b, green shadowed; note that the left and right sides of the shadowed region are spurious peaks from the EPR cavity),

which are quite different from those measured with amorphous films (peaks at 2700-3800 G, the same as frozen solution shown in Figure 1a). The spectrum can be simulated to have two g factors of 2.79 and 2.70, which are originated from the bulk and surface magnetization, respectively, 16 indicating the low temperature ferromagnetism of the single crystal. When rotating the single crystal (0° to 90° to 180°), isotropic behavior was unexpectedly observed; i.e., no change in spectra was observed (Figure 2a, green shadowed), indicating free reorientation of the crystal with the applied magnetic field. However, when the single crystal was fixed by the frozen nonsolvent, the spectrum recorded at 90° rotation demonstrated the as-expected differences from 0° to 90° and a recovery at 180° (Figure 2b, green), confirming the physical reorientation of the free crystal during the measurement in Figure 2a. The single crystal also exhibits EPR hysteresis when applying upward (low to high field) and downward scans (Figure 2c), which again agrees with the ferromagnetic behavior (e.g., at 5 K). As to the microcrystals of $[{\rm Au}_{25}({\rm SR})_{18}]^0$, superparamagnetism is observed below 100 K, and hysteresis becomes perceivable below 40 K (Figure 2d). ¹⁶

The solid-state magnetism of $[Au_{25}(SR)_{18}]^0$ also exhibited some distinct effects of the -R groups of the thiolate ligands, in which the superatomic spin coupling was controlled by the interparticle distance due to the -R groups. For example, using a C_4H_9 group (shorter than CH_2CH_2Ph), Maran's group observed an antiferromagnetic coupling of the superatomic spins of $[Au_{25}(SC_4H_9)_{18}]^0$ NCs, 72 as opposed to the ferromagnetic coupling in the $[Au_{25}(SC_2H_4Ph)_{18}]^0$ assembled solids.

3. MAGNETISM OF DOPED 25-ATOM NANOCLUSTERS AND RELATED SYSTEMS

As mentioned in the previous section, the spherical $[Au_{25}(SR)_{18}]^0$ (SR = SC_2H_4Ph) is the first and foremost case in studying the magnetic properties of Au NCs. The g values of (2.56, 2.36, 1.82) for $[Au_{25}(SR)_{18}]^0$ (frozen solution) significantly shift from g = 2 for the free electron, as well as the values for the single gold atom adsorbed on MgO(001) in

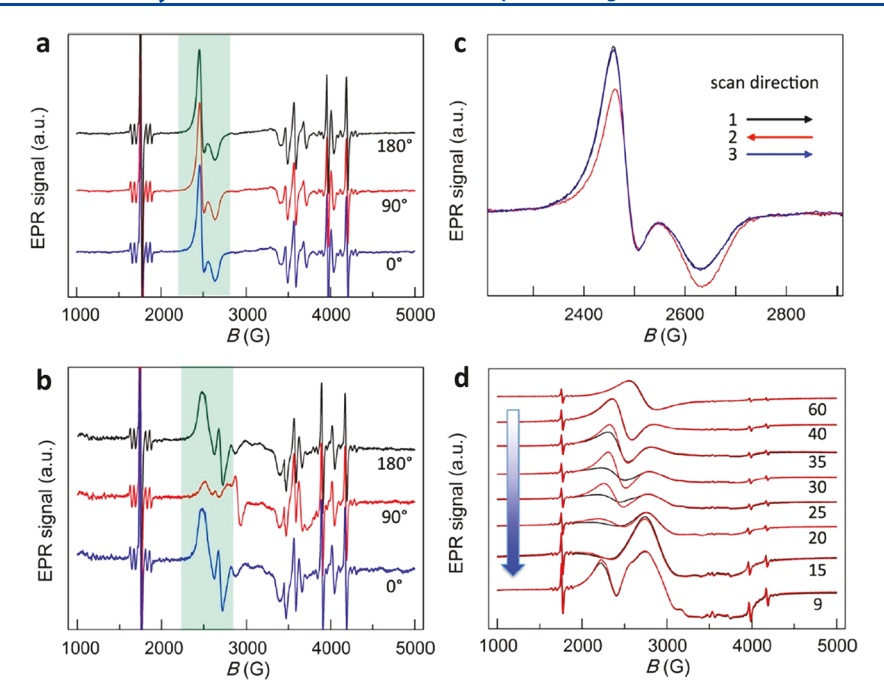


Figure 2. Orientation dependent EPR spectra of a single crystal of $\left[Au_{25}(SR)_{18}\right]^{0}$ (a) free or (b) immobilized by frozen CH₃CN. Note that the left and right sides of the shadowed region are spurious peaks. (c) Hysteresis EPR spectra for a $[Au_{25}(SR)_{18}]^0$ single crystal, T=5 K. (d) Hysteresis EPR spectra of a large collection of $[Au_{25}(SR)_{18}]^0$ microcrystals measured from 60 to 9 K, in which the black and the red traces indicate the upward and downward scans, respectively. Reproduced with permission from ref 16. Copyright 2017, American Chemical Society.

which $g_{\parallel}=1.99$ and $g_{\perp}=2.07.^{73}$ Note that these g values indicate the geometric differences of the spins, i.e., the free electron and the isolated Au⁰ atom have isotropic and axial spin, respectively, while the spin of $[Au_{25}(SR)_{18}]^{\tilde{0}}$ is rhombic, i.e., $g_x \neq g_y \neq g_z$. Other groups later reproduced the EPR spectrum of the same NC, suggesting that it is not necessary to elucidate the EPR data based on 13 equivalent $I = \frac{3}{2}$ ¹⁹⁷Au nuclei because smaller numbers (2, 4, 6, 8 and 10) of equivalent Au atoms do not appreciably affect the simulation due to the anisotropic hyperfine structure.⁷⁴ When the temperature increases from 6 to 50 K, the g values do not change, but the EPR intensity decreases according to the Curie law and the line broadens due to spin relaxation. 57,74 At higher temperatures (>100 K), there is significant broadening in EPR spectra, and no EPR signal is detectable at room temperature.⁵⁷ Another $[Au_{25}(SR')_{18}]^0$ with alkyl thiol $(SR' = SC_2H_5)$ also demonstrates a similar EPR spectrum.⁷⁵

DFT simulations on the isotropic hyperfine coupling constant (A_{iso}) for $[Au_{25}(SR)_{18}]^0$ indicate that, although the Aiso of central Au is only 1.5 MHz and those of the 12 Au atoms in staple motifs are lower than 12.5 MHz, the atoms in the icosahedral Au_{12} shell possess A_{iso} values in the range of 36.0 to 56.4 MHz.⁵⁷ The spin density was also calculated, finding that the staple Au atoms do not share much of the spin density; instead, the spin density is mainly distributed on the icosahedral Au₁₃ kernel.⁵⁷ However, DFT calculations by Kumar and co-workers indicate a controversial result that the spin density is larger on the surface motifs than in the kernel.⁷⁶

In order to obtain more insights into the spin properties of $[Au_{25}(SR)_{18}]^0$, doping heteroatoms into the structure is an effective way. The Pt or Pd doping has been reported to change the electronic structure of the superatom, 77-81 and in the meantime, the magnetic properties could be altered. Experimentally, the central doping of Pt generally results in diamagnetic [PtAu₂₄(SR)₁₈]⁰ (6e, here Pt adopts 6s⁰) and the

electron-shell-closed $[PtAu_{24}(SR)_{18}]^{2-}$ (8e), and the former can be reduced with a large excess of H⁻ to the latter. Interestingly, the Tsukuda group reported that, by reacting $[PtAu_{24}(SR)_{18}]^0$ with 1 equiv of NaBH₄, $[PtAu_{24}(SR)_{18}]^2$ could be obtained, and as the NC has 7e, it is paramagnetic and EPR active.⁸² The EPR spectrum of [PtAu₂₄(SR)₁₈]⁻ shows a rhombic signal (Figure 3) with g values (2.57, 2.37,

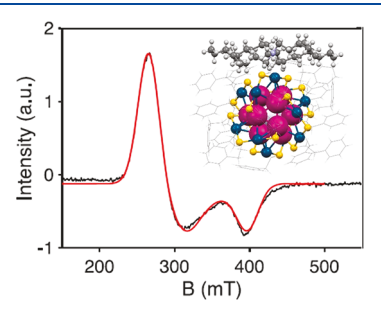


Figure 3. EPR spectrum of $[PtAu_{24}(SC_2H_4Ph)_{18}]^-[N(n-C_8H_{17})_4]^+$ (black = experiment; red = simulation), inset: the total structure of the nanocluster. Color codes: light gray = Pt; magenta = kernel Au; blue = surface motif Au; yellow = S; gray = C; white = H. Reproduced with permission from ref 82. Copyright 2019, American Chemical Society.

1.75), very close to those reported for $[Au_{25}(SR)_{18}]^0$ (see Figure 1a, g = (2.56, 2.36, 1.82). This result not only indicates that [PtAu₂₄(SR)₁₈] is a radical species but also suggests that the spin density on the central Pt⁰ in the 7e (PtAu₁₂)⁵⁺ kernel is almost the same as that on the central gold atom in the 7e (Au₁₃)⁶⁺ kernel.⁸²

Regarding the Pt-related EPR studies, in previous work Roduner et al. studied the three different magnetic states of superatomic Pt₁₃ (most likely with the icosahedral geometry) NCs in details.⁸³ Due to the local environmental differences, NCs in details.83

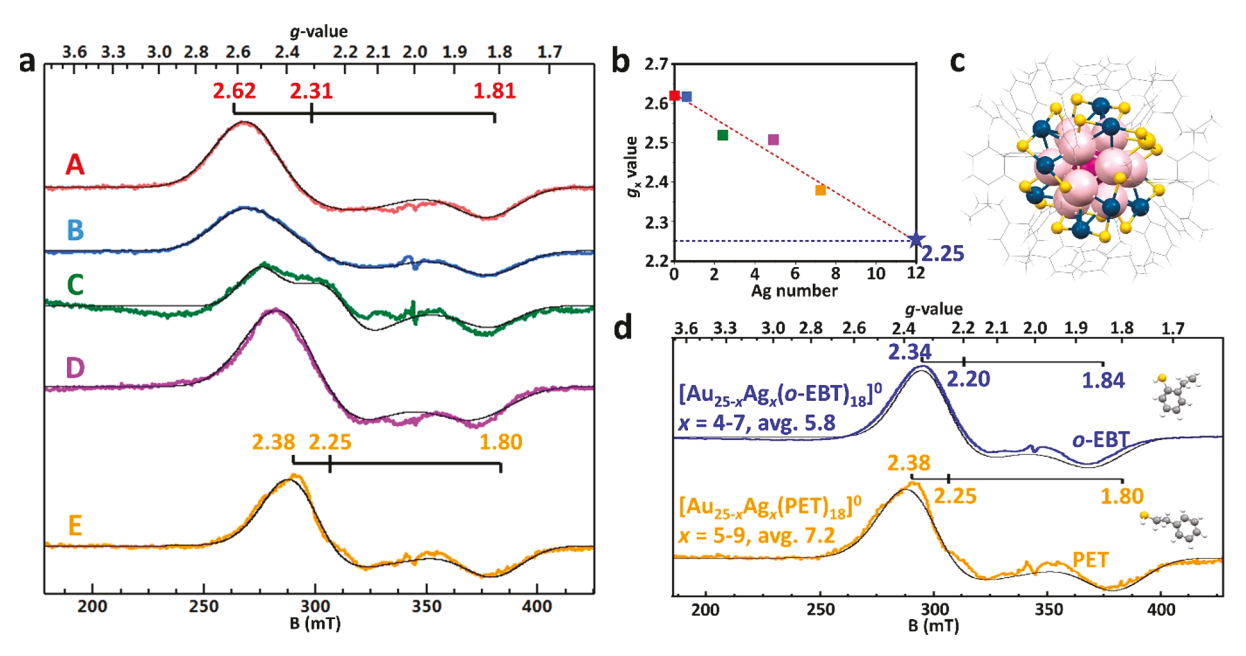


Figure 4. (a) X-band (9.645 GHz) EPR spectra measured at 16 K of $[Au_{25-x}Ag_x(SC_2H_4Ph)_{18}]^0$ with Ag dopant x = (A) 0, (B) 0–2, (C) 0–6, (D) 3–7, and (E) 5–9; microwave power 0.2 mW. (b) Plot of g_x vs the average Ag dopant number in $Au_{25-x}Ag_x$ (or the $Au_{12-x}Ag_x$ shell since the center and exterior staple motifs contain gold exclusively) with maximum x possibly being 12 and the corresponding linear fit. (c) Crystal structure of $[Au_{25-x}Ag_x(SPh-o-C_2H_5)_{18}]^0$ (average x = 5.8). (d) Comparison of the X-band EPR spectra of $[Au_{25-x}Ag_x(SPh-o-C_2H_5)_{18}]^0$ (x = 4-7, average 5.8) with y = (2.34, 2.25, 1.84) and $[Au_{25-x}Ag_x(SC_2H_4Ph)_{18}]^0$ (x = 5-9, average 7.2) with y = (2.38, 2.25, 1.80). Color codes: magenta = central Au; pink = icosahedral shell Au/Ag; blue = surface motif Au; yellow = S; gray = C; white = H. Reproduced with permission from ref 90. Copyright 2020, American Chemical Society.

the NCs are composed of 15-20% with high-spin magnetic moments, < 1% with EPR signal, and the rest is diamagnetic. ⁸⁴ The adsorption and amount of hydrogen (or deuterium) coverage on Pt₁₃ NCs have great effects on the EPR spectra, and EPR signals disappear upon hydrogen desorption. ^{85,86} Moreover, the spectrum of Pt₁₃D_x NCs showing hyperfine splitting can be simulated based on 12 equivalent Pt nuclei (195 Pt, $I = ^{1}/_{2}$, 33.8% natural abundance), and the authors used the superatom picture to describe the undetectably small hyperfine coupling of the central Pt atom (i.e., a very small spin density on the central Pt). ⁸⁵ Thus, the result can be used to support the observation that the spin property of [PtAu₂₄(SR)₁₈]⁻ is the same as that of [Au₂₅(SR)₁₈]⁰, as the Pt doping at the center affects little on the spin density distribution.

By contrast, the paramagnetic property of $\{Ag_{13}[Fe(CO)_4]_8\}^{4-}$ with a cuboctahedral Ag_{13} kernel demonstrates a different story. Each of the doublet line (due to two isotopes of Ag, i.e., ^{107}Ag , $I=^1/_2$, 51.35% natural abundance; ^{109}Ag , $I=^1/_2$, 48.65% natural abundance) is further splitting into 13 observable hyperfine lines. As there is a significant difference between the coupling constants of the central Ag and the Ag atoms in the cuboctahedral Ag_{12} shell, Albano et al. contribute the unpaired electron mainly to the central Ag. The reason that the cluster with Au_{13} kernel has its spin on the shell while the cluster with Ag_{13} kernel has its spin at the center still remains unclear. The different elements, i.e., Au vs Ag, and the different kernel structures, i.e., icosahedral Au_{13} vs cuboctahedral Ag_{13} , might contribute to the significant difference.

Despite the yet unclear difference between Ag and Au, doping silver into $\left[\mathrm{Au}_{25}(\mathrm{SR})_{18}\right]^0$ could be a promising strategy to demonstrate a different picture compared to the Pt doping. However, it has been found that Ag cannot be doped into the central site of the spherical Au_{25} . Nevertheless, the effect

of Ag doping on the EPR signal is still very informative. Jin and co-workers recently reported the manipulation of EPR via controlling the Ag/Au molar ratios in the precursors to obtain a series of $[Au_{25-x}Ag_x(SC_2H_4Ph)_{18}]^0$ (x = 0-9), and the Xband (9.645 GHz) EPR spectra were recorded at 16 K (Figure 4a). The g-tensors of the species with different Ag doping amounts are determined (simulations overlaid on the data), in which the determined g = (2.62, 2.31, 1.81) for [Au₂₅(SC₂H₄Ph)₁₈]⁰ (Figure 4a, sample A) is consistent with that in the previous report⁵⁷ except the slightly different simulation (i.e., the exclusion of a hyperfine term); the same gvalues can be obtained if hyperfine is included. Interestingly, the EPR analysis indicates a clear gradual shift in g-values (g_x) and g_v) for the Ag-doped NCs in comparison to the homogold counterpart (Figure 4a); e.g., for $[Au_{25-x}Ag_x(SC_2H_4Ph)_{18}]^0$ (x = 5-9, average 7.2), g_x and g_y values decrease to 2.38 and 2.25 (sample E). The spin—orbit coupling of the unpaired electron delocalized over the metal atoms in bonding is identified to be responsible for the anisotropic g-tensor, and the decreasing splitting in g_x and g_y with Ag doping can be understood by the much greater spin-orbit coupling parameter of Au (~14400 cm⁻¹) compared to that of Ag (~3470 cm⁻¹). The EPR signals are broadened, as the doped samples (B-E) are mixtures of multiple species. The plot of g_x vs the average number of Ag in [Au_{25-x}Ag_x(SC₂H₄Ph)₁₈]⁰ gives a linear trend and $g_x = 2.25$ at the maximum x of 12 (Figure 4b), i.e., all of the atoms in the icosahedral shell are Ag. The exclusion of Ag at the center, as well as the exterior staple motif sites, is proved by SCXRD of $[Au_{25-x}Ag_x(SPh-o-C_2H_5)_{18}]^0$ (x = 4-7, average 5.8, Figure 4c). Since the SPh-o-C₂H₅ ligand is the aromatic homologue of SC₂H₄Ph. A comparative EPR study on axial splitting in Ag-doped systems shows that the carbon tail isomerism in the thiolate ligand also has some effect on the magnetic properties (Figure 4d). $[Au_{25-x}Ag_x(SPh-o-C_2H_5)_{18}]^0$

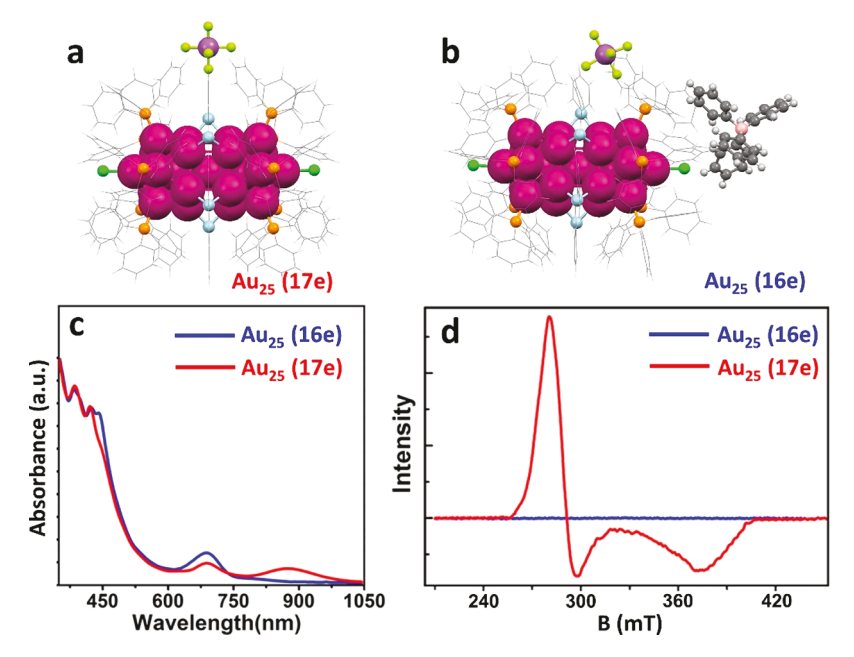


Figure 5. Total structures of (a) $[Au_{25}(PPh_3)_{10}(SePh)_5Cl_2]^+(SbF_6)^-$ (17e) and (b) $[Au_{25}(PPh_3)_{10}(SePh)_5Cl_2]^{2+}(SbF_6)^-$ (16e). (c) UV-vis absorption spectra of (blue) Au_{25} (16e) and (red) Au_{25} (17e). (d) EPR spectra of (blue) Au_{25} (16e) and (red) Au_{25} (17e). Both spectra were recorded at 5 K (microwave frequency, 9.4 GHz; microwave power, 25 μ W; amplitude modulation, 0.5 mT). Color codes: magenta = Au; orange = P; light blue = Se; green = Cl; gray = C; white = H. Reproduced with permission from ref 100. Copyright 2016, American Chemical Society.

showed a slight reduction in axial splitting in comparison to $[Au_{25-x}Ag_x(SC_2H_4Ph)_{18}]^0$. This may be contributed by aromatic vs nonaromatic ligand systems⁹² and the interactions between the metal kernel and the capping ligands.⁹³

4. MAGNETISM IN THE Au₂₅-ROD NANOCLUSTER

Compared to the spherical $\mathrm{Au}_{25}(\mathrm{SR})_{18}$ NC, the rod-shaped $[\mathrm{Au}_{25}(\mathrm{PPh}_3)_{10}(\mathrm{SR})_5\mathrm{Cl}_2]^{2+}$ NC is also well studied, including the synthesis, structure, luminescence, electrochemistry, and ultrafast dynamics. He structure of rod-shaped Au_{25} contains two icosahedral Au_{13} units connected via sharing a vertex gold atom (Figure 5a,b). According to Mingos' electron counting rule as well as the ligand protection of $[\mathrm{Au}_{25}(\mathrm{PPh}_3)_{10}(\mathrm{SR})_5\mathrm{Cl}_2]^{2+}$, the valence electron number is 16 (i.e., 25-5-2-2=16e). Note that the phosphine ligands adopt dative bonds and do not contribute to the electron count. Thus, the rod-shaped Au_{25} NC can be considered to be two 8e superatoms combined together.

Based on the rod-shaped Au₂₅, Song et al. replaced the thiolates with selenolate (SePh) and studied the magnetic properties of [Au₂₅(PPh₃)₁₀(SePh)₅Cl₂]^q by controlling the number of counterions (Figure 5), including Au₂₅ (17e) when q = 1+, counterion = SbF₆, and Au₂₅ (16e) when q = 2+, counterions = one SbF₆ and one BPh₄ according to SCXRD. 100 After reacting with H₂O₂ (10%), the rod-shaped Au₂₅ (17e) can be oxidized to Au₂₅ (16e) as indicated by time-dependent UV-vis absorption spectra, in which the peak at 870 nm disappears and the 420 nm peak divides into two shoulder peaks (Figure 5c). By contrast, the Au₂₅ (16e) cannot be reduced back to Au₂₅ (17e) by excess NaBH₄, suggesting that the formation of Au₂₅ (17e) is obtained by kinetic control. The Au₂₅ (16e) sample is EPR silent due to the even number of electrons (Figure 5d, blue line), like the thiolate counterpart $[Au_{25}(PPh_3)_{10}(SR)_5Cl_2]^{2+}$. Interestingly, the Au_{25} (17e) microcrystal powders measured at 5 K demonstrates a strong EPR signal with $S = \frac{1}{2}$, g = (2.40, 2.26, 1.78) (Figure 5d, red line).

This is different from the signal observed for a spherical $[\mathrm{Au}_{25}(\mathrm{SC}_2\mathrm{H}_4\mathrm{Ph})_{18}]^0$ with g=(2.56,2.36,1.82). Although both Au NCs contain 25 gold atoms, their structures and protecting ligands are different. The $[\mathrm{Au}_{25}(\mathrm{PPh}_3)_{10}(\mathrm{SePh})_5\mathrm{Cl}_2]^+$ (17e) case consolidates the conclusion that for Au NPs of ultrasmall sizes, the exact electron count determined by their precise formulas can serve as an indicator for magnetism. Besides this, the EPR signal provides further evidence for that the charge of Au_{25} (17e) is +1 as determined by SCXRD, as it is possible that small counterion(s) might not be resolved by SCXRD.

5. MAGNETISM IN THE Au₁₃₃ NANOCLUSTER

In addition to the small-sized Au NCs discussed above, larger Au NCs with unpaired electron have also been reported 101 and are even more intriguing as these NCs bridge up the small NCs possessing discrete energy levels with conventional plasmonic NPs possessing a quasi-continuous band. 102,103 The magnetism of atomically precise Au_n(SR)_m NCs can serve as an important indicator for the investigation on the transition from atomic magnetism (localized) to delocalized spin to band magnetism. Among the Au NCs of large sizes (>100 atoms of Au), the charge-neutral Au₁₃₃(SR)₅₂ (81e) of 1.7 nm core diameter is a recent example, which illustrates a different EPR spectrum from that of $\mathrm{Au}_{25}(\mathrm{SR})_{18}$ (7e). Both the S- and X-band spectra of $\text{Au}_{133}(\text{SR})_{52}$ display a signal with $g_{\parallel} = 2.47$ and $g_{\perp} =$ 1.69 (Figure 6a). As the EPR signal intensity is temperaturedependent from 2 to 25 K, obeying the Curie law (intensity vs 1/T), the behavior of magnetism in atomically precise Au₁₃₃(SR)₅₂ is different from the temperature-independent, electron-conduction-band Pauli paramagnetism. EPR quantitation of Au₁₃₃(SR)₅₂ reveals that each NC possesses one unpaired spin. Electron loss (i.e., oxidation by H₂O₂) results in an EPR inactive $[Au_{133}(SR)_{52}]^+$ (80e) NC (Figure 6a, green line). A comparison of EPR signals between Au₁₃₃(SR)₅₂ and Au₂₅(SR)₁₈ clearly shows that the shape of magnetic moment for the former is axial, while the latter is rhombic (Figure 6b).

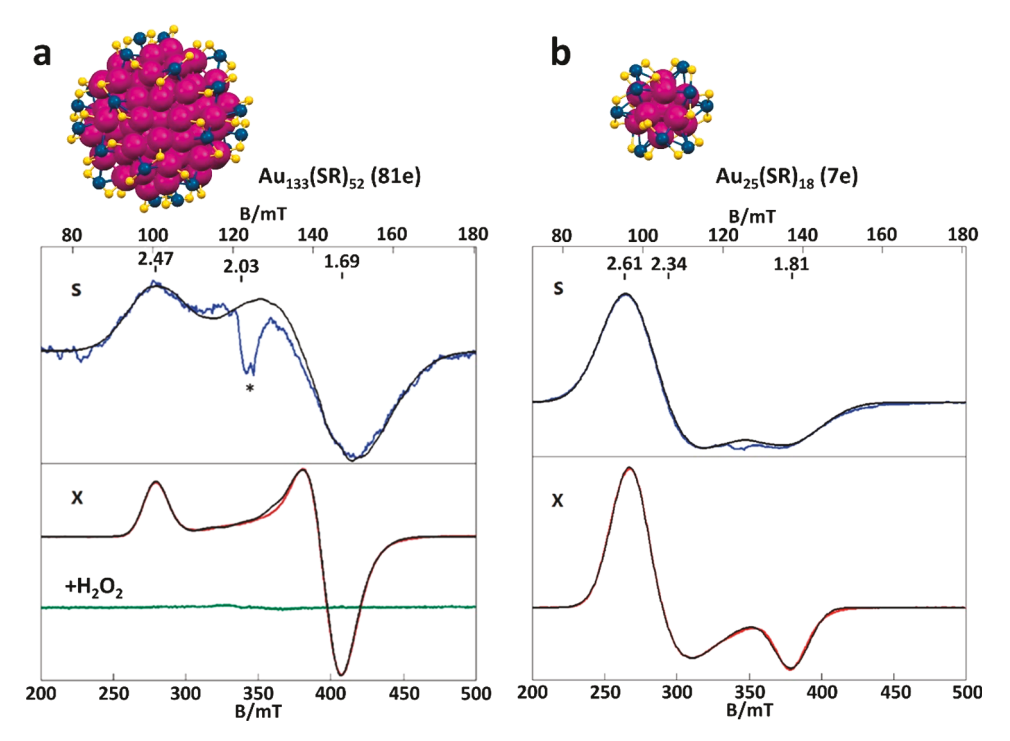


Figure 6. S-band (3.48 GHz) at 10 K and X-band (9.64 GHz) at 6 K EPR spectra (blue/black lines) of (a) $Au_{133}(SR)_{52}$ and (b) $Au_{25}(SR)_{18}$ dissolved in toluene/CH₂Cl₂, v:v = 1:1. Microwave power: 0.3 mW (S-band); 2 mW (X-band). The green trace shows loss of EPR signal after H₂O₂ oxidation. The signal at g = 2.03 signal (marked with *) comes from the copper impurity. Smooth lines are simulations. The structures of (a) $Au_{133}S_{52}$ and (b) $Au_{25}S_{18}$ (-R groups omitted for clarity) are also shown. Color codes: magenta = kernel Au; blue = motif Au; yellow = S. Reproduced with permission from ref 101. Copyright 2019, The Royal Society of Chemistry.

If we take the average of the two larger g values of $\mathrm{Au}_{25}(\mathrm{SR})_{18}$, the axial tensors become $g_{\parallel}=1.81$ and $g_{\perp}=2.48$, and the directions of the g tensors are in reverse in comparison to $\mathrm{Au}_{133}(\mathrm{SR})_{52}$, indicating a change in the symmetry of the unpaired electron. The simulations for $\mathrm{Au}_{133}(\mathrm{SR})_{52}$ indicate a spin of $\mathrm{S}=^{1}/_{2}$ with 12 equivalent Au nuclei with $A_{\mathrm{iso}}=50$ MHz. These parameters are comparable to those of $\mathrm{Au}_{25}(\mathrm{SR})_{18}$, i.e., the unpaired electron is delocalized on the innermost icosahedral Au_{12} shell.

The above-discussed cases of EPR activity have common character that the spherical Au_{25} , rod-shaped Au_{25} , and spherical Au_{133} , all contain icosahedral kernel structures. The number of electrons in these icosahedral $Au_n(SR)_m$ NCs can be readily altered by oxidation/reduction, and the spin is likely distributed on the icosahedral Au_{12} shell that wraps the central atom.

6. FUTURE PERSPECTIVES

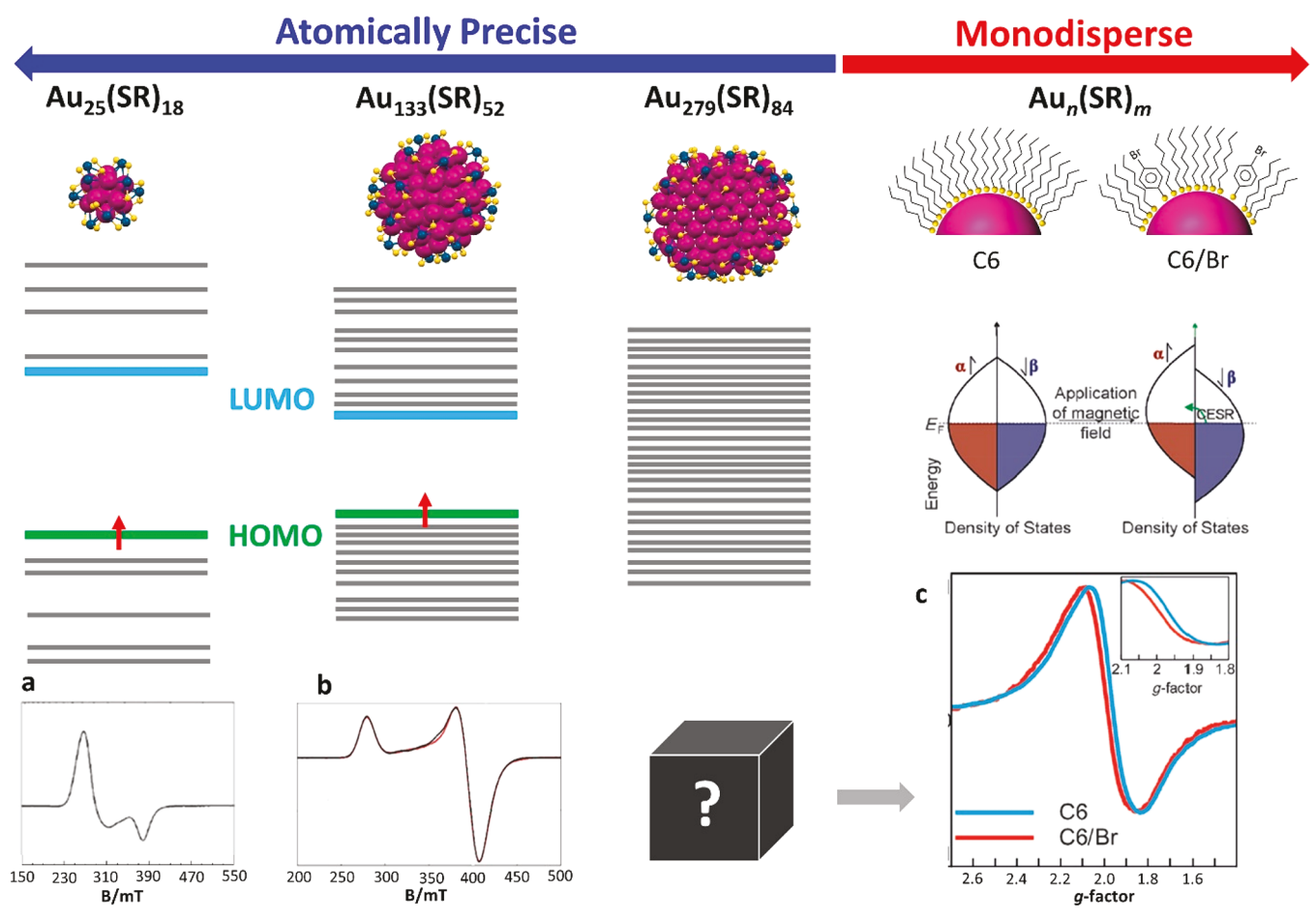
While bulk Au is diamagnetic, Au NPs may exhibit interesting magnetic properties, especially in the 1-4 nm regime. The magnetic studies on regular NPs that are imprecise and with possible impurities still cannot reach a consistent conclusion. Therefore, the development of atomically precise Au NCs (Scheme 1a,b) provide a great opportunity for mechanistic studies, as all of the particles are truly identical in size and structure, such as the classic case of $[Au_{25}(SR)_{18}]^0$ (7e), which clearly reveals that each particle holds one unpaired spin with axial splitting of the g value. The NC can be reversibly reduced to diamagnetic $[Au_{25}(SR)_{18}]^-$ (8e, EPR inactive). Based on the chemical formula (i.e., the numbers of metal atoms, ligands and charges), one can directly tell if the NC is paramagnetic or not. For conventional NPs, as the exact electron count cannot

be determined due to nonuniformity of the NPs and no atomic precision, it is only possible to relate the magnetism to the NP size.³ Note that the EPR active NCs reported so far are still small in size and possess molecular-like electronic structure only, and their energy gaps are larger than the thermal energy.¹⁰¹ When the size approaches the metallic state, thermal energy and the increasing population of electrons lying beneath the excited states are expected to present some interesting phenomena, which deserves future studies.

A vast majority of atomically precise metal NCs turn out to have even numbers of valence electrons, and even if the metal-ligand number subtraction indicates an odd number, the open-shelled electronic structure and the natural pairing requirement (especially for small-sized NCs) would often lead to a charge in the NC for eliminating the magnetism, and subsequently the counterion(s) associate with these NCs according to the positive or negative state of the NC. 104 In order to have a more complete picture on the spin delocalization and the effect of geometry on the signal profile, more EPR-active NCs need to be created via size and chargestate control. When the size increases, the geometrical structure becomes more important for the stability of NCs than does the electronic structure. Interestingly, unlike homogold NCs, alloy NCs tend to bear charges, e.g., [Au₃Ag₃₈(SR)₂₄X₅]²⁻(PPh₄)₂²⁺ (X = Cl, Br), ¹⁰⁸ [Au₂₄-Ag₄₆(SR)₃₂]²⁺(BPh₄)²⁻, ¹⁰⁶ [Cu₃₀Ag₆₁(SR)₃₈S₃]⁺(BPh₄)⁻, ¹⁰⁷ and Au₅₂Cu₇₂(SR)₅₅⁺(SbF₆)⁻. EPR activity could be achieved by controlling the electron binding. 109 Recent work shows that $[Au_{18}Cu_{32}(SR)_{36}]^{2-}$ containing an icosahedral Au_{12} kernel can be reduced to $[Au_{18}Cu_{32}(SR)_{36}]^{3-}$ which displays a strong EPR signal with $S = \frac{1}{2}$ and g = (2.02, 2.35).

Some cases on Ag NCs have also been reported to be EPR active, 111-114 but no doublet signal from 107Ag and 109Ag

Scheme 1. Gold NCs with Schematic Energy States and the Corresponding EPR Spectra of (a) Au₂₅(SR)₁₈, (b) Au₁₃₃(SR)₅₂, and Au₂₇₉(SR)₈₄ and (c) a Schematic of the Pauli Paramagnetism of Au-SR NPs^b and the Corresponding CESR Spectra^c



^aIts EPR spectrum is unknown as yet. ^bPart c has Au-SR NPs protected by (left) *n*-hexanethiolate (C6 for short) and (right) partially modified with 4-bromobenzenthiolate (C6/Br). ^cPanel a: Reproduced with permission from ref 57. Copyright 2009, American Chemical Society. Panel b: Reproduced with permission from ref 101. Copyright 2019, The Royal Society of Chemistry. Panel c: Reproduced with permission from ref 102. Copyright 2015, Wiley-VCH Verlag GmbH & Co. KGaA, Weinheim.

(51:49) was observed, except an isotropic EPR profile. This is probably due to the broadening (overlap) of the signal, as seen in Au analogues. It is worth mentioning that although $\mathrm{Au}_{25}(\mathrm{SR})_{18}$ (7e) and its alloy NCs have been studied in terms of paramagnetism, its silver analog, i.e., $[\mathrm{Ag}_{25}(\mathrm{SR})_{18}]^{-,115}$ has no success yet in oxidization to 7e. It has been demonstrated that Au doping is able to enhance the stability and photoluminescence of Ag_{25} , 116 and we suppose that the doped Ag_{25} could also be a good candidate to study the EPR of Ag NCs. Overall, systematic EPR measurements and quantitative analysis are necessary in order to have an unambiguous assignment of EPR signals and eliminate the possibility of impurities in future work.

The magnetic NCs observed so far all belong to the molecular state with a sizable HOMO–LUMO gap (as opposed to plasmonic NPs with zero gap). As to conventional NPs, the strength of Au–S charge transfer localizes surface conduction electrons in plasmonic NPs, affecting the width of surface plasmonic resonance (SPR). ¹¹⁷ In metallic Au-SR NPs, electrons are arranged in quasi-continuous states, and CESR can be used to detect the magnetic properties of the metallic electrons near the Fermi level. The signal is very sensitive to ligand tailoring (Scheme 1c). ¹⁰² Interestingly, an abrupt

transition was observed from the molecular-state $Au_{246}(SR)_{80}$ to the metallic/plasmonic $Au_{279}(SR)_{84}$. ¹¹⁸ The $Au_{279}(SR)_{84}$ NC has 195e, which is an odd number, and thus, it would be interesting to study its magnetic properties. This will help understand the magnetic transition from the molecular state to the metallic state (Scheme 1a–c). Similarly, $Au_{191}(SR)_{66}$ with 125e is another potentially interesting case to study in future work. ¹¹⁹

The structural dependence of magnetism in Au NCs is also an interesting aspect and remains to be investigated. As we discussed in the above sections, Au NCs with icosahedral kernels are generally found to be more facile in adding/removing one electron for imparting magnetism, while those with fcc structures tends to accept/lose 2e with structural evolution. Thus, more work is needed to explore and engineer the nonicosahedral Au NCs for fundamental understanding and magnetic functionality expansion.

The use of heteroatoms as dopants for the EPR active NCs can be quite valuable for probing the spin delocalization inside the Au NCs. For example, similar to the case of spherical ${\rm Au_{25-x}Ag_x}$ systems, Ag doping in the rod-shaped ${\rm Au_{25}}$ (17e) may show a significant effect on the ERP signal, which could be carried out in future work. In addition, as it has been clear

that the spin is delocalized in the icosahedral $\mathrm{Au_{12}}$ shell of spherical $\mathrm{Au_{25}(SR)_{18}}$ and ligands are directly anchored on this shell, ligand tailoring might also have some effect on the magnetic properties and is worth studying in the future. Previous experiments on Au NPs have demonstrated that different types of ligands, e.g., thiolate vs amine, could effectively alter the SPR, electron—phonon coupling and magnetic properties of the NPs. 122 As the recently developed alkynyl-protected Au NCs are thriving in their sizes and applications, 123 and some of them share the same structures as Au-SR NCs, 124 it would be interesting to compare them in respect to EPR signals.

Overall, magnetism in gold and other metal nanoclusters, as well as the doped or alloy nanoclusters, will continue to be an intriguing topic, and future research is expected to obtain further control over the spin properties in isolated particles and to understand exchange coupling between particles in the assembled solids. The superparamagnetic, antiferromagnetic, and ferromagnetic states of the nanocluster-assembled solids remain to be investigated, and based on that, the characteristic temperatures (such as the blocking temperature and the Néel temperature) may acquire an exquisite tuning. Both the isolated nanoclusters and the assembled solids with versatile magnetic functionality 125,126 will find applications in sensing, catalysis, and quantum technology.

AUTHOR INFORMATION

Corresponding Author

Rongchao Jin — Department of Chemistry, Carnegie Mellon University, Pittsburgh, Pennsylvania 15213, United States; orcid.org/0000-0002-2525-8345; Email: rongchao@andrew.cmu.edu

Author

Yingwei Li — Department of Chemistry, Carnegie Mellon University, Pittsburgh, Pennsylvania 15213, United States; orcid.org/0000-0002-4813-6009

Complete contact information is available at: https://pubs.acs.org/10.1021/acs.jpcc.1c04621

Notes

The authors declare no competing financial interest.

Biographies

Yingwei Li received her B.S. and M.S. in condensed matter physics from Shanghai Normal University (Shanghai, China) and joined Prof. Rongchao Jin's group in 2016. Her research focuses on the syntheses, structures, and properties of atomically precise gold and alloy nanoclusters.

Rongchao Jin is Professor of Chemistry at Carnegie Mellon University. He received his B.S. in Chemical Physics from USTC in 1995, his M.S. in Physical Chemistry/Catalysis from Dalian Institute of Chemical Physics in 1998, and his Ph.D. in Chemistry from Northwestern University in 2003. After his postdoctoral research at the University of Chicago, he joined the chemistry faculty of CMU in 2006. His research interests include atomically precise nanoparticles, optics of nanoparticles, and catalysis.

ACKNOWLEDGMENTS

We thank Saborni Biswas for helpful discussions during the preparation of the manuscript. R.J. acknowledges the NSF funding (DMR-1808675).

REFERENCES

- (1) Sommers, C. B.; Amar, H. Relativistic Band Structure of Gold. *Phys. Rev.* **1969**, *188*, 1117–1120.
- (2) White, R. M. Quantum Theory of Magnetism, 3rd ed.; Springer: New York, 2007.
- (3) Wu, Z.; Chen, J.; Jin, R. One-Pot Synthesis of Au₂₅(SG)₁₈ ²⁻ and 4-nm Gold Nanoparticles and Comparison of Their Size-Dependent Properties. *Adv. Funct. Mater.* **2011**, *21*, 177–183.
- (4) Halperin, W. P. Quantum Size Effects in Metal Particles. Rev. Mod. Phys. 1986, 58, 533-606.
- (5) Hori, H.; Teranishi, T.; Nakae, Y.; Seino, Y.; Miyake, M.; Yamada, S. Anomalous Magnetic Polarization Effect of Pd and Au Nano-Particles. *Phys. Lett. A* **1999**, 263, 406–410.
- (6) Nealon, G. L.; Donnio, B.; Greget, R.; Kappler, J.-P.; Terazzi, E.; Gallani, J.-L. Magnetism in Gold Nanoparticles. *Nanoscale* **2012**, *4*, 5244–5258.
- (7) Tuboltsev, V.; Savin, A.; Pirojenko, A.; Räisänen, J. Magnetism in Nanocrystalline Gold. *ACS Nano* **2013**, *7*, 6691–6699.
- (8) Yamamoto, Y.; Miura, T.; Suzuki, M.; Kawamura, N.; Miyagawa, H.; Nakamura, T.; Kobayashi, K.; Teranishi, T.; Hori, H. Direct Observation of Ferromagnetic Spin Polarization in Gold Nanoparticles. *Phys. Rev. Lett.* **2004**, *93*, 116801.
- (9) Crespo, P.; Litrán, R.; Rojas, T. C.; Multigner, M.; de la Fuente, J. M.; Sánchez-López, J. C.; García, M. A.; Hernando, A.; Penadés, S.; Fernández, A. Permanent Magnetism, Magnetic Anisotropy, and Hysteresis of Thiol-Capped Gold Nanoparticles. *Phys. Rev. Lett.* **2004**, 93, 087204.
- (10) Hernando, A.; Crespo, P.; García, M. A. Origin of Orbital Ferromagnetism and Giant Magnetic Anisotropy at the Nanoscale. *Phys. Rev. Lett.* **2006**, *96*, 057206.
- (11) Guerrero, E.; Muñoz-Márquez, M. A.; García, M. A.; Crespo, P.; Fernández-Pinel, E.; Hernando, A.; Fernández, A. Surface Plasmon Resonance and Magnetism of Thiol-Capped Gold Nanoparticles. *Nanotechnology* **2008**, *19*, 175701.
- (12) Dutta, P.; Pal, S.; Seehra, M. S.; Anand, M.; Roberts, C. B. Magnetism in Dodecanethiol-Capped Gold Nanoparticles: Role of Size and Capping Agent. *Appl. Phys. Lett.* **2007**, *90*, 213102.
- (13) Muñoz-Márquez, M. A.; Guerrero, E.; Fernández, A.; Crespo, P.; Hernando, A.; Lucena, R.; Conesa, J. C. Permanent Magnetism in Phosphine- and Chlorine-Capped Gold: From Clusters to Nanoparticles. *J. Nanopart. Res.* **2010**, *12*, 1307–1318.
- (14) Hori, H.; Yamamoto, Y.; Iwamoto, T.; Miura, T.; Teranishi, T.; Miyake, M. Diameter Dependence of Ferromagnetic Spin Moment in Au Nanocrystals. *Phys. Rev. B: Condens. Matter Mater. Phys.* **2004**, *69*, 174411.
- (15) He, L. Comment on Diameter Dependence of Ferromagnetic Spin Moment in Au Nanocrystals". *Phys. Rev. B: Condens. Matter Mater. Phys.* **2010**, *81*, 096401.
- (16) Agrachev, M.; Antonello, S.; Dainese, T.; Ruzzi, M.; Zoleo, A.; Aprà, E.; Govind, N.; Fortunelli, A.; Sementa, L.; Maran, F. Magnetic Ordering in Gold Nanoclusters. *ACS Omega* **2017**, *2*, 2607–2617.
- (17) Cirri, A.; Silakov, A.; Jensen, L.; Lear, B. J. Probing Ligand-Induced Modulation of Metallic States in Small Gold Nanoparticles Using Conduction Electron Spin Resonance. *Phys. Chem. Chem. Phys.* **2016**, *18*, 25443–25451.
- (18) Cirri, A.; Silakov, A.; Jensen, L.; Lear, B. J. Chain Length and Solvent Control over the Electronic Properties of Alkanethiolate-Protected Gold Nanoparticles at the Molecule-to-Metal Transition. *J. Am. Chem. Soc.* **2016**, *138*, 15987–15993.
- (19) Jin, R.; Zeng, C.; Zhou, M.; Chen, Y. Atomically Precise Colloidal Metal Nanoclusters and Nanoparticles: Fundamentals and Opportunities. *Chem. Rev.* **2016**, *116*, 10346–10413.
- (20) Chakraborty, I.; Pradeep, T. Atomically Precise Clusters of Noble Metals: Emerging Link between Atoms and Nanoparticles. *Chem. Rev.* **2017**, *117*, 8208–8271.
- (21) Alvarez, M. M.; Khoury, J. T.; Schaaff, T. G.; Shafigullin, M. N.; Vezmar, I.; Whetten, R. L. Optical Absorption Spectra of Nanocrystal Gold Molecules. *J. Phys. Chem. B* **1997**, *101*, 3706–3712.

- (22) Zhou, M.; Higaki, T.; Li, Y.; Zeng, C.; Li, Q.; Sfeir, M. Y.; Jin, R. Three-Stage Evolution from Nonscalable to Scalable Optical Properties of Thiolate-Protected Gold Nanoclusters. *J. Am. Chem. Soc.* **2019**, *141*, 19754–19764.
- (23) Zhou, M.; Higaki, T.; Hu, G.; Sfeir, M. Y.; Chen, Y.; Jiang, D.; Jin, R. Three-Orders-of-Magnitude Variation of Carrier Lifetimes with Crystal Phase of Gold Nanoclusters. *Science* **2019**, *364*, 279–282.
- (24) Higaki, T.; Li, Q.; Zhou, M.; Zhao, S.; Li, Y.; Li, S.; Jin, R. Toward the Tailoring Chemistry of Metal Nanoclusters for Enhancing Functionalities. *Acc. Chem. Res.* **2018**, *51*, 2764–2773.
- (25) Li, Y.; Luo, T.-Y.; Zhou, M.; Song, Y.; Rosi, N. L.; Jin, R. A Correlated Series of Au/Ag Nanoclusters Revealing the Evolutionary Patterns of Asymmetric Ag Doping. *J. Am. Chem. Soc.* **2018**, *140*, 14235–14243.
- (26) Li, Y.; Cowan, M. J.; Zhou, M.; Luo, T.-Y.; Song, Y.; Wang, H.; Rosi, N. L.; Mpourmpakis, G.; Jin, R. Atom-by-Atom Evolution of the Same Ligand-Protected Au₂₁, Au₂₂, Au₂₂Cd₁, and Au₂₄ Nanocluster Series. J. Am. Chem. Soc. **2020**, 142, 20426–20433.
- (27) Li, Y.; Taylor, M. G.; Luo, T.-Y.; Song, Y.; Rosi, N. L.; Mpourmpakis, G.; Jin, R. Heteroatom Tracing Reveals the 30-Atom Au-Ag Bimetallic Nanocluster as a Dimeric Structure. *J. Phys. Chem. Lett.* **2020**, *11*, 7307–7312.
- (28) Zeng, C.; Chen, Y.; Kirschbaum, K.; Lambright, K. J.; Jin, R. Emergence of Hierarchical Structural Complexities in Nanoparticles and Their Assembly. *Science* **2016**, 354, 1580–1584.
- (29) Higaki, T.; Liu, C.; Zhou, M.; Luo, T.-Y.; Rosi, N. L.; Jin, R. Tailoring the Structure of 58-Electron Gold Nanoclusters: $Au_{103}S_2(S-Nap)_{41}$ and Its Implications. *J. Am. Chem. Soc.* **2017**, *139*, 9994–10001.
- (30) Li, Y.; Jin, R. Seeing Ligands on Nanoclusters and in Their Assemblies by X-Ray Crystallography: Atomically Precise Nanochemistry and Beyond. *J. Am. Chem. Soc.* **2020**, *142*, 13627–13644.
- (31) Chen, Y.; Liu, C.; Tang, Q.; Zeng, C.; Higaki, T.; Das, A.; Jiang, D.-e.; Rosi, N. L.; Jin, R. Isomerism in Au28(SR)20 Nanocluster and Stable Structures. *J. Am. Chem. Soc.* **2016**, *138*, 1482–1485.
- (32) Tian, S.; Li, Y.-Z.; Li, M.-B.; Yuan, J.; Yang, J.; Wu, Z.; Jin, R. Structural Isomerism in Gold Nanoparticles Revealed by X-Ray Crystallography. *Nat. Commun.* **2015**, *6*, 8667.
- (33) Liu, X.; Xu, W. W.; Huang, X.; Wang, E.; Cai, X.; Zhao, Y.; Li, J.; Xiao, M.; Zhang, C.; Gao, Y.; et al. De Novo Design of $\mathrm{Au}_{36}(\mathrm{SR})_{24}$ Nanoclusters. *Nat. Commun.* **2020**, *11*, 3349.
- (34) Li, Y.; Zhou, M.; Jin, R. Programmable Metal Nanoclusters with Atomic Precision. *Adv. Mater.* **2021**, 2006591.
- (35) Zhou, M.; Zeng, C.; Chen, Y.; Zhao, S.; Sfeir, M. Y.; Zhu, M.; Jin, R. Evolution from the Plasmon to Exciton State in Ligand-Protected Atomically Precise Gold Nanoparticles. *Nat. Commun.* **2016**, *7*, 13240.
- (36) Zhou, M.; Jin, R. Optical Properties and Excited-State Dynamics of Atomically Precise Gold Nanoclusters. *Annu. Rev. Phys. Chem.* **2021**, *72*, 121–142.
- (37) Li, Y.; Higaki, T.; Du, X.; Jin, R. Chirality and Surface Bonding Correlation in Atomically Precise Metal Nanoclusters. *Adv. Mater.* **2020**, 32, 1905488.
- (38) Pelayo, J. J.; Valencia, I.; García, A. P.; Chang, L.; López, M.; Toffoli, D.; Stener, M.; Fortunelli, A.; Garzón, I. L. Chirality in Bare and Ligand-Protected Metal Nanoclusters. *Adv. Phys-X* **2018**, 3, 1509727.
- (39) Nieto-Ortega, B.; Bürgi, T. Vibrational Properties of Thiolate-Protected Gold Nanoclusters. Acc. Chem. Res. 2018, 51, 2811–2819.
- (40) Kang, X.; Zhu, M. Tailoring the Photoluminescence of Atomically Precise Nanoclusters. *Chem. Soc. Rev.* **2019**, 48, 2422–2457.
- (41) Song, Y.; Li, Y.; Zhou, M.; Liu, X.; Li, H.; Wang, H.; Shen, Y.; Zhu, M.; Jin, R. Ultrabright Au@Cu₁₄ Nanoclusters: 71.3% Phosphorescence Quantum Yield in Non-Degassed Solution at Room Temperature. *Sci. Adv.* **2021**, *7*, No. eabd2091.
- (42) Goswami, N.; Yao, Q.; Luo, Z.; Li, J.; Chen, T.; Xie, J. Luminescent Metal Nanoclusters with Aggregation-Induced Emission. *J. Phys. Chem. Lett.* **2016**, *7*, 962–975.

- (43) Li, Y.; Cowan, M. J.; Zhou, M.; Taylor, M. G.; Wang, H.; Song, Y.; Mpourmpakis, G.; Jin, R. Heterometal-Doped M_{23} (M = Au/Ag/Cd) Nanoclusters with Large Dipole Moments. ACS Nano 2020, 14, 6599–6606.
- (44) Li, Y.; Chen, Y.; House, S. D.; Zhao, S.; Wahab, Z.; Yang, J. C.; Jin, R. Interface Engineering of Gold Nanoclusters for CO Oxidation Catalysis. ACS Appl. Mater. Interfaces 2018, 10, 29425–29434.
- (45) Higaki, T.; Li, Y.; Zhao, S.; Li, Q.; Li, S.; Du, X.-S.; Yang, S.; Chai, J.; Jin, R. Atomically Tailored Gold Nanoclusters for Catalytic Application. *Angew. Chem., Int. Ed.* **2019**, *58*, 8291–8302.
- (46) Jin, R.; Li, G.; Sharma, S.; Li, Y.; Du, X. Toward Active-Site Tailoring in Heterogeneous Catalysis by Atomically Precise Metal Nanoclusters with Crystallographic Structures. *Chem. Rev.* **2021**, *121*, 567–648.
- (47) Li, S.; Nagarajan, A. V.; Li, Y.; Kauffman, D. R.; Mpourmpakis, G.; Jin, R. The Role of Ligands in Atomically Precise Nanocluster-Catalyzed CO₂ Electrochemical Reduction. *Nanoscale* **2021**, *13*, 2333–2337.
- (48) Agrachev, M.; Ruzzi, M.; Venzo, A.; Maran, F. Nuclear and Electron Magnetic Resonance Spectroscopies of Atomically Precise Gold Nanoclusters. *Acc. Chem. Res.* **2019**, *52*, 44–52.
- (49) Trudel, S. Unexpected Magnetism in Gold Nanostructures: Making Gold Even More Attractive. *Gold Bull.* **2011**, *44*, 3–13.
- (50) Singh, R. Unexpected Magnetism in Nanomaterials. *J. Magn. Magn. Mater.* **2013**, 346, 58–73.
- (51) Hembury, M.; Chiappini, C.; Bertazzo, S.; Kalber, T. L.; Drisko, G. L.; Ogunlade, O.; Walker-Samuel, S.; Krishna, K. S.; Jumeaux, C.; Beard, P.; et al. Gold-Silica Quantum Rattles for Multimodal Imaging and Therapy. *Proc. Natl. Acad. Sci. U. S. A.* **2015**, *112*, 1959–1964.
- (52) Zhang, P.; Sham, T. K. X-Ray Studies of the Structure and Electronic Behavior of Alkanethiolate-Capped Gold Nanoparticles: The Interplay of Size and Surface Effects. *Phys. Rev. Lett.* **2003**, *90*, 245502.
- (53) Zhang, Z.; Berg, A.; Levanon, H.; Fessenden, R. W.; Meisel, D. On the Interactions of Free Radicals with Gold Nanoparticles. *J. Am. Chem. Soc.* **2003**, *125*, 7959–7963.
- (54) Niermann, N.; Degefa, T. H.; Walder, L.; Zielke, V.; Steinhoff, H.-J.; Onsgaard, J.; Speller, S. Galvinoxyl Monolayers on Au(111) Studied by STM, EPR, and Cyclic Voltammetry. *Phys. Rev. B: Condens. Matter Mater. Phys.* **2006**, 74, 235424.
- (55) Mannini, M.; Sorace, L.; Gorini, L.; Piras, F. M.; Caneschi, A.; Magnani, A.; Menichetti, S.; Gatteschi, D. Self-Assembled Organic Radicals on Au(111) Surfaces: A Combined ToF-SIMS, STM, and ESR Study. *Langmuir* 2007, 23, 2389–2397.
- (56) Mas-Torrent, M.; Crivillers, N.; Rovira, C.; Veciana, J. Attaching Persistent Organic Free Radicals to Surfaces: How and Why. *Chem. Rev.* **2012**, *112*, 2506–2527.
- (57) Zhu, M.; Aikens, C. M.; Hendrich, M. P.; Gupta, R.; Qian, H.; Schatz, G. C.; Jin, R. Reversible Switching of Magnetism in Thiolate-Protected Au25 Superatoms. *J. Am. Chem. Soc.* **2009**, *131*, 2490–2492.
- (58) Negishi, Y.; Chaki, N. K.; Shichibu, Y.; Whetten, R. L.; Tsukuda, T. Origin of Magic Stability of Thiolated Gold Clusters: A Case Study on Au₂₅(SC₆H₁₃)₁₈. *J. Am. Chem. Soc.* **2007**, *129*, 11322–11323.
- (59) Walter, M.; Akola, J.; Lopez-Acevedo, O.; Jadzinsky, P. D.; Calero, G.; Ackerson, C. J.; Whetten, R. L.; Grönbeck, H.; Häkkinen, H. A Unified View of Ligand-Protected Gold Clusters as Superatom Complexes. *Proc. Natl. Acad. Sci. U. S. A.* **2008**, *105*, 9157–9162.
- (60) Aikens, C. M. Origin of Discrete Optical Absorption Spectra of $M_{25}(SH)_{18}^-$ Nanoparticles (M = Au, Ag). *J. Phys. Chem. C* **2008**, 112, 19797–19800.
- (61) Jadzinsky, P. D.; Calero, G.; Ackerson, C. J.; Bushnell, D. A.; Kornberg, R. D. Structure of a Thiol Monolayer-Protected Gold Nanoparticle at 1.1 Å Resolution. *Science* **2007**, *318*, 430–433.
- (62) Yang, H.; Wang, Y.; Huang, H.; Gell, L.; Lehtovaara, L.; Malola, S.; Häkkinen, H.; Zheng, N. All-Thiol-Stabilized Ag₄₄ and Au₁₂Ag₃₂ Nanoparticles with Single-Crystal Structures. *Nat. Commun.* **2013**, *4*, 2422.

- (63) Akola, J.; Walter, M.; Whetten, R. L.; Häkkinen, H.; Grönbeck, H. On the Structure of Thiolate-Protected Au₂₅. *J. Am. Chem. Soc.* **2008**, *130*, 3756–3757.
- (64) Zhu, M.; Eckenhoff, W. T.; Pintauer, T.; Jin, R. Conversion of Anionic [Au₂₅(SCH₂CH₂Ph)₁₈]⁻ Cluster to Charge Neutral Cluster via Air Oxidation. *J. Phys. Chem. C* **2008**, *112*, 14221–14224.
- (65) Aikens, C. M. Geometric and Electronic Structure of $Au_{25}(SPhX)_{18}^-$ (X = H, F, Cl, Br, CH₃, and OCH₃). *J. Phys. Chem. Lett.* **2010**, *1*, 2594–2599.
- (66) Jiang, D.; Kühn, M.; Tang, Q.; Weigend, F. Superatomic Orbitals under Spin-Orbit Coupling. *J. Phys. Chem. Lett.* **2014**, *5*, 3286–3289.
- (67) Zhu, M.; Aikens, C. M.; Hollander, F. J.; Schatz, G. C.; Jin, R. Correlating the Crystal Structure of a Thiol-Protected Au₂₅ Cluster and Optical Properties. *J. Am. Chem. Soc.* **2008**, *130*, 5883–5885.
- (68) Tofanelli, M. A.; Salorinne, K.; Ni, T. W.; Malola, S.; Newell, B.; Phillips, B.; Häkkinen, H.; Ackerson, C. J. Jahn-Teller Effects in Au₂₅(SR)₁₈. *Chem. Sci.* **2016**, *7*, 1882–1890.
- (69) Gutrath, B. S.; Englert, U.; Wang, Y.; Simon, U. A Missing Link in Undecagold Cluster Chemistry: SingleCrystal X-Ray Analysis of [Au₁₁(PPh₃)₇Cl₃]. *Eur. J. Inorg. Chem.* **2013**, 2013, 2002–2006.
- (70) McKenzie, L. C.; Zaikova, T. O.; Hutchison, J. E. Structurally Similar Triphenylphosphine-Stabilized Undecagolds, Au₁₁(PPh₃)₇Cl₃ and [Au₁₁(PPh₃)₈Cl₂]Cl, Exhibit Distinct Ligand Exchange Pathways with Glutathione. *J. Am. Chem. Soc.* **2014**, *136*, 13426–13435.
- (71) Akbari-Sharbaf, A.; Hesari, M.; Workentin, M. S.; Fanchini, G. Electron Paramagnetic Resonance in Positively Charged Au₂₅ Molecular Nanoclusters. *J. Chem. Phys.* **2013**, *138*, 024305.
- (72) De Nardi, M.; Antonello, S.; Jiang, D.-e.; Pan, F.; Rissanen, K.; Ruzzi, M.; Venzo, A.; Zoleo, A.; Maran, F. Gold Nanowired: A Linear $(Au_{25})_n$ Polymer from Au_{25} Molecular Clusters. *ACS Nano* **2014**, 8, 8505–8512
- (73) Yulikov, M.; Sterrer, M.; Heyde, M.; Rust, H.-P.; Risse, T.; Freund, H.-J.; Pacchioni, G.; Scagnelli, A. Binding of Single Gold Atoms on Thin MgO(001) Films. *Phys. Rev. Lett.* **2006**, *96*, 146804.
- (74) Antonello, S.; Perera, N. V.; Ruzzi, M.; Gascón, J. A.; Maran, F. Interplay of Charge State, Lability, and Magnetism in the Molecule-like Au₂₅(SR)₁₈ Cluster. *J. Am. Chem. Soc.* **2013**, *135*, 15585–15594.
- (75) Dainese, T.; Antonello, S.; Gascón, J. A.; Pan, F.; Perera, N. V.; Ruzzi, M.; Venzo, A.; Zoleo, A.; Rissanen, K.; Maran, F. Au₂₅(SEt)₁₈, a Nearly Naked Thiolate-Protected Au₂₅ Cluster Structural Analysis by Single Crystal X-ray Crystallography and Electron Nuclear Double Resonance. *ACS Nano* **2014**, *8*, 3904–3912.
- (76) Krishna, K. S.; Tarakeshwar, P.; Mujica, V.; Kumar, C. S. S. R. Chemically Induced Magnetism in Atomically Precise Gold Clusters. *Small* **2014**, *10*, 907–911.
- (77) Qian, H.; Jiang, D.; Li, G.; Gayathri, C.; Das, A.; Gil, R. R.; Jin, R. Monoplatinum Doping of Gold Nanoclusters and Catalytic Application. *J. Am. Chem. Soc.* **2012**, *134*, 16159–16162.
- (78) Kauffman, D. R.; Alfonso, D.; Matranga, C.; Qian, H.; Jin, R. A Quantum Alloy: The Ligand-Protected Au_{25-x}Ag_x(SR)₁₈ Cluster. *J. Phys. Chem. C* **2013**, *117*, 7914–7923.
- (79) Kwak, K.; Tang, Q.; Kim, M.; Jiang, D.; Lee, D. Interconversion between Superatomic 6-Electron and 8-Electron Configurations of $M@Au_{24}(SR)_{18}$ Clusters (M = Pd, Pt). J. Am. Chem. Soc. **2015**, 137, 10833–10840.
- (80) Hossain, S.; Niihori, Y.; Nair, L. V.; Kumar, B.; Kurashige, W.; Negishi, Y. Alloy Clusters: Precise Synthesis and Mixing Effects. *Acc. Chem. Res.* **2018**, *51*, 3114–3124.
- (81) Kang, X.; Li, Y.; Zhu, M.; Jin, R. Atomically Precise Alloy Nanoclusters: Syntheses, Structures, and Properties. *Chem. Soc. Rev.* **2020**, *49*, 6443–6514.
- (82) Suyama, M.; Takano, S.; Nakamura, T.; Tsukuda, T. Stoichiometric Formation of Open-Shell $[PtAu_{24}(SC_2H_4Ph)_{18}]^-$ via Spontaneous Electron Proportionation between $[PtAu_{24}(SC_2H_4Ph)_{18}]^{2-}$ and $[PtAu_{24}(SC_2H_4Ph)_{18}]^{0-}$. J. Am. Chem. Soc. **2019**, 141, 14048–14051.
- (83) Roduner, E.; Jensen, C.; van Slageren, J.; Rakoczy, R. A.; Larlus, O.; Hunger, M. Anomalous Diamagnetic Susceptibility in 13-Atom

- Platinum Nanocluster Superatoms. Angew. Chem., Int. Ed. 2014, 53, 4318-4321.
- (84) Bartolomé, J.; Bartolomé, F.; García, L. M.; Roduner, E.; Akdogan, Y.; Wilhelm, F.; Rogalev, A. Magnetization of Pt₁₃ Clusters Supported in a NaY Zeolite: A XANES and XMCD Study. *Phys. Rev. B: Condens. Matter Mater. Phys.* **2009**, *80*, 014404.
- (85) Roduner, E.; Jensen, C. Magnetic Properties and the Superatom Character of 13-Atom Platinum Nanoclusters. *Magneto-chemistry* **2015**, *1*, 28–44.
- (86) Jensen, C.; van Slageren, J.; Jakes, P.; Eichel, R.-A.; Roduner, E. Support Effects on Hydrogen Desorption, Isotope Exchange, Chemical Reactivity, and Magnetism of Platinum Nanoclusters in KL Zeolite. *J. Phys. Chem. C* 2013, *117*, 22732–22745.
- (87) Albano, V. G.; Grossi, L.; Longoni, G.; Monari, M.; Mulley, S.; Sironi, A. Synthesis and Characterization of the Paramagnetic [Ag₁₃Fe₈(CO)₃₂]⁴ Tetraanion: A Cuboctahedral Ag₁₃ Cluster Stabilized by Fe(CO)₄ Groups Behaving as 4-Electron Donors. *J. Am. Chem. Soc.* **1992**, *114*, 5708–5713.
- (88) Kumara, C.; Aikens, C. M.; Dass, A. X-Ray Crystal Structure and Theoretical Analysis of Au_{25-x}Ag_x(SCH₂CH₂Ph)₁₈ Alloy. *J. Phys. Chem. Lett.* **2014**, *5*, 461–466.
- (89) Li, Q.; Wang, S.; Kirschbaum, K.; Lambright, K. J.; Das, A.; Jin, R. Heavily Doped $Au_{25-x}Ag_x(SC_6H_{11})_{18}^-$ Nanoclusters: Silver Goes from the Core to the Surface. *Chem. Commun.* **2016**, *52*, 5194–5197.
- (90) Li, Y.; Biswas, S.; Luo, T.-Y.; Juarez-Mosqueda, R.; Taylor, M. G.; Mpourmpakis, G.; Rosi, N. L.; Hendrich, M. P.; Jin, R. Doping Effect on the Magnetism of Thiolate-Capped 25-Atom Alloy Nanoclusters. *Chem. Mater.* **2020**, 32, 9238–9244.
- (91) Martin, W. C. Table of Spin-Orbit Energies for *p*-Electrons in Neutral Atomic (Core) np Configurations. *J. Res. Natl. Bur. Stand., Sect. A* **1971**, *75A*, 109–111.
- (92) Li, Y.; Juarez-Mosqueda, R.; Song, Y.; Zhang, Y.; Chai, J.; Mpourmpakis, G.; Jin, R. Ligand Exchange on Au₃₈(SR)₂₄: Substituent Site Effects of Aromatic Thiols. *Nanoscale* **2020**, *12*, 9423–9429.
- (93) Agrachev, M.; Antonello, S.; Dainese, T.; Gascón, J. A.; Pan, F.; Rissanen, K.; Ruzzi, M.; Venzo, A.; Zoleo, A.; Maran, F. A Magnetic Look into the Protecting Layer of Au₂₅ Clusters. *Chem. Sci.* **2016**, *7*, 6910–6918.
- (94) Shichibu, Y.; Negishi, Y.; Watanabe, T.; Chaki, N. K.; Kawaguchi, H.; Tsukuda, T. Biicosahedral Gold Clusters $[\mathrm{Au}_{25}(\mathrm{PPh}_3)_{10}(\mathrm{SC}_n\mathrm{H}_{2n+1})_5\mathrm{Cl}_2]^{2+}$ (n=2-18): A Stepping Stone to Cluster-Assembled Materials. J. Phys. Chem. C **2007**, 111, 7845–7847.
- (95) Qian, H.; Eckenhoff, W. T.; Bier, M. E.; Pintauer, T.; Jin, R. Crystal Structures of Au₂ Complex and Au₂₅ Nanocluster and Mechanistic Insight into the Conversion of Polydisperse Nanoparticles into Monodisperse Au₂₅ Nanoclusters. *Inorg. Chem.* **2011**, *50*, 10735–10739.
- (96) Sfeir, M. Y.; Qian, H.; Nobusada, K.; Jin, R. Ultrafast Relaxation Dynamics of Rod-Shaped 25-Atom Gold Nanoclusters. *J. Phys. Chem.* C **2011**, *115*, 6200–6207.
- (97) Wang, S.; Meng, X.; Das, A.; Li, T.; Song, Y.; Cao, T.; Zhu, X.; Zhu, M.; Jin, R. A 200-Fold Quantum Yield Boost in the Photoluminescence of Silver Doped Ag_xAu_{25-x} Nanoclusters: The 13th Silver Atom Matters. *Angew. Chem., Int. Ed.* **2014**, *53*, 2376–2380
- (98) Zhao, S.; Austin, N.; Li, M.; Song, Y.; House, S. D.; Bernhard, S.; Yang, J. C.; Mpourmpakis, G.; Jin, R. Influence of Atomic-Level Morphology on Catalysis: The Case of Sphere and Rod-Like Gold Nanoclusters for CO₂ Electroreduction. *ACS Catal.* **2018**, *8*, 4996–5001.
- (99) Chen, S.; Ma, H.; Padelford, J. W.; Qinchen, W.; Yu, W.; Wang, S.; Zhu, M.; Wang, G. Near Infrared Electrochemiluminescence of Rod-Shape 25-Atom AuAg Nanoclusters That Is Hundreds-Fold Stronger Than That of Ru(Bpy)₃ Standard. *J. Am. Chem. Soc.* **2019**, 141, 9603–9609.
- (100) Song, Y.; Jin, S.; Kang, X.; Xiang, J.; Deng, H.; Yu, H.; Zhu, M. How a Single Electron Affects the Properties of the "Non-Superatom" Au₂₅ Nanoclusters. *Chem. Mater.* **2016**, *28*, 2609–2617.

- (101) Zeng, C.; Weitz, A.; Withers, G.; Higaki, T.; Zhao, S.; Chen, Y.; Gil, R. R.; Hendrich, M.; Jin, R. Controlling Magnetism of Au₁₃₃(TBBT)₅₂ Nanoclusters at Single Electron Level and Implication for Nonmetal to Metal Transition. *Chem. Sci.* **2019**, *10*, 9684–9691.
- (102) Cirri, A.; Silakov, A.; Lear, B. J. Ligand Control over the Electronic Properties within the Metallic Core of Gold Nanoparticles. *Angew. Chem., Int. Ed.* **2015**, *54*, 11750–11753.
- (103) Cruz, S. S.; Tanygin, V.; Lear, B. J. Asymmetries in the Electronic Properties of Spheroidal Metallic Nanoparticles, Revealed by Conduction Electron Spin Resonance and Surface Plasmon Resonance. ACS Nano 2021, 15, 4490–4503.
- (104) Das, A.; Li, T.; Nobusada, K.; Zeng, C.; Rosi, N. L.; Jin, R. Nonsuperatomic $[Au_{23}(SC_6H_{11})_{16}]^-$ Nanocluster Featuring Bipyramidal Au_{15} Kernel and Trimeric $Au_3(SR)_4$ Motif. *J. Am. Chem. Soc.* **2013**, *135*, 18264–18267.
- (105) Wang, Z.; Senanayake, R.; Aikens, C. M.; Chen, W.-M.; Tung, C.-H.; Sun, D. Gold-Doped Silver Nanocluster $[Au_3Ag_{38}(SCH_2Ph)_{24}X_5]^{2-}$ (X = Cl or Br). Nanoscale **2016**, 8, 18905–18911.
- (106) Wang, S.; Jin, S.; Yang, S.; Chen, S.; Song, Y.; Zhang, J.; Zhu, M. Total Structure Determination of Surface Doping [Ag₄₆Au₂₄(SR)₃₂](BPh₄)₂ Nanocluster and Its Structure-Related Catalytic Property. *Sci. Adv.* **2015**, *1*, No. e1500441.
- (107) Zou, X.; Li, Y.; Jin, S.; Kang, X.; Wei, X.; Wang, S.; Meng, X.; Zhu, M. Doping Copper Atoms into the Nanocluster Kernel: Total Structure Determination of [Cu₃₀Ag₆₁(SAdm)₃₈S₃](BPh₄). *J. Phys. Chem. Lett.* **2020**, *11*, 2272–2276.
- (108) Song, Y.; Li, Y.; Li, H.; Ke, F.; Xiang, J.; Zhou, C.; Li, P.; Zhu, M.; Jin, R. Atomically Resolved $Au_{52}Cu_{72}(SR)_{55}$ Nanoalloy Reveals Marks Decahedron Truncation and Penrose Tiling Surface. *Nat. Commun.* **2020**, *11*, 478.
- (109) Tasaka, Y.; Nakamura, K.; Malola, S.; Hirata, K.; Kim, K.; Koyasu, K.; Häkkinen, H.; Tsukuda, T. Electron Binding in a Superatom with a Repulsive Coulomb Barrier: The Case of $[Ag_{44}(SC_6H_3F_2)_{30}]^4$ in the Gas Phase. *J. Phys. Chem. Lett.* **2020**, 11. 3069–3074.
- (110) Li, Q.; Chai, J.; Yang, S.; Song, Y.; Chen, T.; Chen, C.; Zhang, H.; Yu, H.; Zhu, M. Multiple Ways Realizing Charge-State Transform in Au-Cu Bimetallic Nanoclusters with Atomic Precision. *Small* **2021**, 17, 1907114
- (111) Liu, C.; Li, T.; Abroshan, H.; Li, Z.; Zhang, C.; Kim, H. J.; Li, G.; Jin, R. Chiral Ag₂₃ Nanocluster with Open Shell Electronic Structure and Helical Face-Centered Cubic Framework. *Nat. Commun.* **2018**, *9*, 744.
- (112) Liu, X.; Chen, J.; Yuan, J.; Li, Y.; Li, J.; Zhou, S.; Yao, C.; Liao, L.; Zhuang, S.; Zhao, Y.; Deng, H.; Yang, J.; Wu, Z. A Silver Nanocluster Containing Interstitial Sulfur and Unprecedented Chemical Bonds. *Angew. Chem.* **2018**, *130*, 11443–11447.
- (113) Xi, X.-J.; Yang, J.-S.; Wang, J.-Y.; Dong, X.-Y.; Zang, S.-Q. New Stable Isomorphous Ag₃₄ and Ag₃₃Au Nanoclusters with an Open Shell Electronic Structure. *Nanoscale* **2018**, *10*, 21013–21018.
- (114) Ma, X.; Bai, Y.; Song, Y.; Li, Q.; Lv, Y.; Zhang, H.; Yu, H.; Zhu, M. Rhombicuboctahedral Ag₁₀₀: Four-Layered Octahedral Silver Nanocluster Adopting the Russian Nesting Doll Model. *Angew. Chem., Int. Ed.* **2020**, *59*, 17234–17238.
- (115) Joshi, C. P.; Bootharaju, M. S.; Alhilaly, M. J.; Bakr, O. M. $[Ag_{25}(SR)_{18}]^-$: The "Golden" Silver Nanoparticle. *J. Am. Chem. Soc.* **2015**, *137*, 11578–11581.
- (116) Ghosh, A.; Mohammed, O. F.; Bakr, O. M. Atomic-Level Doping of Metal Clusters. Acc. Chem. Res. 2018, 51, 3094-3103.
- (117) Garcia, M. A.; de la Venta, J.; Crespo, P.; Llopis, J.; Penadés, S.; Fernández, A.; Hernando, A. Surface Plasmon Resonance of Capped Au Nanoparticles. *Phys. Rev. B: Condens. Matter Mater. Phys.* **2005**, 72, 241403.
- (118) Higaki, T.; Zhou, M.; Lambright, K. J.; Kirschbaum, K.; Sfeir, M. Y.; Jin, R. Sharp Transition from Nonmetallic Au₂₄₆ to Metallic Au₂₇₉ with Nascent Surface Plasmon Resonance. *J. Am. Chem. Soc.* **2018**, *140*, 5691–5695.

- (119) Sakthivel, N. A.; Shabaninezhad, M.; Sementa, L.; Yoon, B.; Stener, M.; Whetten, R. L.; Ramakrishna, G.; Fortunelli, A.; Landman, U.; Dass, A. The Missing Link: Au₁₉₁(SPh-^tBu)₆₆ Janus Nanoparticle with Molecular and Bulk-Metal-like Properties. *J. Am. Chem. Soc.* **2020**, *142*, 15799–15814.
- (120) Xu, W. W.; Zeng, X. C.; Gao, Y. Application of Electronic Counting Rules for Ligand-Protected Gold Nanoclusters. *Acc. Chem. Res.* 2018, *51*, 2739–2747.
- (121) Pei, Y.; Wang, P.; Ma, Z.; Xiong, L. Growth-Rule-Guided Structural Exploration of Thiolate-Protected Gold Nanoclusters. *Acc. Chem. Res.* **2019**, *52*, 23–33.
- (122) Aruda, K. O.; Tagliazucchi, M.; Sweeney, C. M.; Hannah, D. C.; Schatz, G. C.; Weiss, E. A. Identification of Parameters through Which Surface Chemistry Determines the Lifetimes of Hot Electrons in Small Au Nanoparticles. *Proc. Natl. Acad. Sci. U. S. A.* **2013**, *110*, 4212
- (123) Lei, Z.; Wan, X.-K.; Yuan, S.-F.; Guan, Z.-J.; Wang, Q.-M. Alkynyl Approach toward the Protection of Metal Nanoclusters. *Acc. Chem. Res.* **2018**, *51*, 2465–2474.
- (124) Li, J.-J.; Guan, Z.-J.; Lei, Z.; Hu, F.; Wang, Q.-M. Same Magic Number but Different Arrangement: Alkynyl-Protected Au_{25} with D_3 Symmetry. *Angew. Chem., Int. Ed.* **2019**, *58*, 1083–1087.
- (125) Lee, C.-H.; Liu, L.; Bejger, C.; Turkiewicz, A.; Goko, T.; Arguello, C. J.; Frandsen, B. A.; Cheung, S. C.; Medina, T.; Munsie, T. J. S.; et al. Ferromagnetic Ordering in Superatomic Solids. *J. Am. Chem. Soc.* **2014**, *136*, 16926–16931.
- (126) Chauhan, V.; Sahoo, S.; Khanna, S. N. Ni₉Te₆(PEt₃)₈C₆₀ Is a Superatomic Superalkali Superparamagnetic Cluster Assembled Material (S₃-CAM). *J. Am. Chem. Soc.* **2016**, *138*, 1916–1921.